Article

Double-Layered Sillen−Aurivillius Perovskite Oxybromide Sr$_2$Bi$_3$Nb$_2$O$_{11}$Br as a Fatigue-Free Piezocatalyst with Ultrahigh Hydrogen Evolution Performance

Published as part of Chemistry of Materials virtual special issue "C. N. R. Rao at 90".

Maqsuma Banoo,[∥] Arjun Kumar Sah,[∥] Raj Sekhar Roy, Pooja Bhardwaj, Digamber G. Porob, Goutam Sheet, and Ujjal K. Gautam*

Cite This: *Chem. Mater.* 2024, 36, 6558−6566

Read Online

ACCESS | Metrics & More | Article Recommendations | Supporting Information

ABSTRACT: Piezocatalytic water splitting is an emerging approach for generating green hydrogen by using noise. However, while the efficiency of hydrogen production remains limited, barely anything is known about the long-term usability of the piezocatalysts. In this study, we present single-crystalline Sr$_2$Bi$_3$Nb$_2$O$_{11}$Br nanoplates with precise facet control and remarkable piezoelectric properties, exhibiting a significantly enhanced piezocatalytic hydrogen production rate of 5.3 mmol/g/h without needing any expensive cocatalyst, such as Pt. Furthermore, we extend the application of these nanoplates to seawater splitting with a commendable rate retention of 4.1 mmol/g/h seawater, mimicking NaCl solution and 3.5 mmol/g/h in real, unprocessed seawater, surpassing the existing piezocatalysts operated using pure water. A key finding in this work is the fatigue-resistant nature of the Sr$_2$Bi$_3$Nb$_2$O$_{11}$Br nanoplates originating from the layered structure. These maintain ~100% activity for over 150 h of continuous operation, while the existing catalysts have not been tested beyond 10−15 h, offering a sustainable approach for renewable hydrogen production.
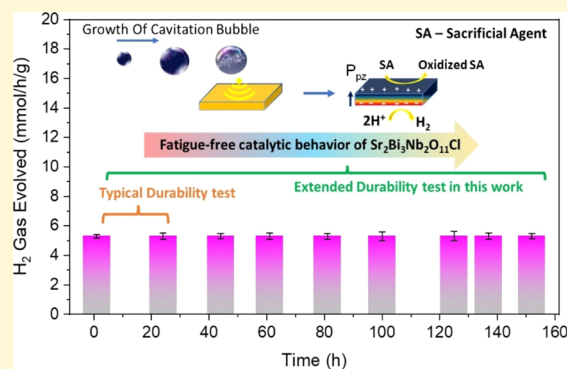
INTRODUCTION

Catalytic water splitting has become increasingly attractive for sustainable energy generation, offering an alternative to fossil fuels, while mitigating challenges from carbon dioxide emissions. This process involves harnessing various renewable energy sources, such as solar light, waste heat, and mechanical vibrations, etc., to produce high-energy-density hydrogen (H$_2$).[1−4] Among emerging technologies, piezocatalytic water splitting, i.e., converting waste mechanical energy, such as ultrasound noise, into chemical energy, stands out for its potential to improve H$_2$ production. This approach leverages piezoelectric materials that can develop surface charges when subjected to external pressure. The piezopotential so developed on the surface across a catalyst particle during ultrasound-induced piezocatalysis can reduce protons, facilitating efficient hydrogen production. Even though a technoeconomic evaluation of this approach is yet not available, piezocatalysis can potentially have several beneficial features as compared to conventional photocatalysis and electrocatalysis.[5−7] Unlike photocatalysis, piezocatalysis does not require precise band-edge positioning, as the piezopotential naturally adjusts the energy levels of the conduction and valence bands, favorable for water splitting. Moreover, piezocatalysis does not necessitate using materials with high

electrical conductivity, a prerequisite for electrocatalysis, thus broadening its applicability in renewable energy production.[8−10]

Furthermore, the vast expanse of the world's oceans, which hold 97% of the Earth's water, presents a unique opportunity for endless production of hydrogen from unprocessed water. The ocean environment encompasses a wide frequency spectrum, including low frequencies generated by shipping activities (10−500 Hz), medium frequencies from sonars (0.5−25 kHz), and high frequencies from thermal noise (>25 kHz), which can serve as renewable sources of pressure for piezocatalytic seawater splitting. This diversity of naturally available frequencies makes piezocatalytic seawater splitting an attractive catalytic approach for hydrogen production. In our previous work, we demonstrated piezocatalytic seawater splitting feasibility, albeit with low efficiency. Therefore, it is
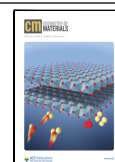
necessary to develop catalysts with enhanced seawater splitting efficiency.[7,11]

Piezoelectric materials have traditionally been used to convert mechanical energy into electrical energy for applications, such as sensors, actuators, and transducers.[12,13] However, it is only recently that researchers have shifted focus toward using such materials for piezocatalytic water splitting. A significant milestone was marked by Hong et al., who demonstrated water splitting using piezoelectric ZnO microfibers and $BaTiO_3$ microdendrites.[14] Since then, several materials, such as $BiFeO_3$, Bi_2WO_6, MoS_2, and BiOCl, have been explored as piezocatalysts for hydrogen production.[11,15,16] Despite notable progress, challenges persist in enhancing the piezocatalysis efficiency and expanding the range of candidate materials.

Additionally, the degradation of catalysts during catalysis is a significant concern that can limit their long-term performance and effectiveness. In photocatalysis, catalyst degradation can occur due to various factors, such as surface oxidation, photocorrosion, and photocatalyst aggregation. Similarly, in electrocatalysis, catalyst degradation can result from processes, such as corrosion, poisoning, and surface restructuring. For instance, Domen et al. explored $Rh_{2-y}Cr_yO_3/GaN/ZnO$ powder for photocatalytic water splitting over a much longer time than the conventional practices and identified the origin of deactivation as surface damage.[17] Similarly, some of us recently explored Pd–Ni alloy nanowires as an efficient electrocatalyst for oxygen reduction for extended use of over 200 K cycles and attributed an activity decrease of 45% to Ni leaching, even though the end-activity is still an order of magnitude higher than the initial activity of commercial Pt/C.[18] To mitigate such catalyst degradation events during renewable energy harvesting, various strategies have been devised involving catalysts' surface modification, the use of protective coatings, employing support materials, etc.[19,20] Investigation on piezocatalysis, on the other hand, is relatively recent, and the stability of piezocatalysts during prolonged use has not received attention so far. Yet, the exploration of the same is critical since sonic energy is known to severely damage materials and is often used to exfoliate layered materials, making the long-term performance of the piezocatalysts questionable. In this context, developing high-performance piezoelectric materials that can be used for a long time is of significance for the realization of sustainable and practically applicable piezocatalysts.

Herein, we present highly active facet-controlled single-crystalline $Sr_2Bi_3Nb_2O_{11}Br$ nanoplates with a relatively high surface area obtained using a single-step flux method, which requires much-simplified synthesis conditions compared to the traditional solid-state synthesis approach. These nanoplates exhibit a remarkably high piezoelectric coefficient of 244 pm/V and piezocatalytic water splitting efficiency, leading to a hydrogen production rate of 5.3 mmol/g/h at a sonar frequency of 37 kHz, without requiring any additional cocatalysts. We further extend the application scope to seawater splitting through piezocatalysis, achieving a hydrogen production rate of 3.5 mmol/g/h in real seawater, which is better than many other piezocatalysts for pure water splitting. A significant attribution of this work is in exploring the long-term usability of a catalyst during piezocatalysis. For the first time, we demonstrate that the $Sr_2Bi_3Nb_2O_{11}Br$ nanoplates with an intrinsic layered structure can sustain continuous ultrasonic treatment for over 150 h, an order of magnitude higher period

than previously examined. During this period, there was negligible change in hydrogen production activity, confirming the fatigue-free nature of the Sillen−Aurivillius phase.

■ RESULTS AND DISCUSSION

The alternating $(Bi_2O_2)^{2+}$ and perovskite $(A_{n-1}B_nO_{3n+1})^{2-}$ layers in Aurivillius compounds have long been known to play a crucial role in the realization of fatigue-resistant ferroelectricity for applications in electrical energy storage. The $(Bi_2O_2)^{2+}$ layers carry net electrical charges, and their arrangement within the lattice is self-adjusted to counter-balance space charges, thereby enhancing the fatigue resistance of the Aurivillius phase.[21−23]

The Sillen−Aurivillius (SA) phases share structural similarities with the Aurivillius phase with the incorporation of an additional halide layer between the $(Bi_2O_2)^{2+}$ layers. These widely studied multiferroic phases can be denoted as $[Bi_2O_2] [A_{n-1}B_nO_{3n+1}] [Bi_2O_2] [X_m]$, where A represents Ca^{2+}, Sr^{2+}, Bi^{3+}, etc., B represents Nb^{5+}, Ta^{5+}, Ti^{4+}, etc., "m" represents the number of halide layers (X), and "n" signifies the number of perovskite layers. SA phases exhibit remarkable structural flexibility emanating from the compositional versatility of cations with varying valences and "n".[24−27]

In this context, structural ambiguity emerging from many studies for varying values of "n" is enticing because when n = 1, these phases can be unequivocally assigned to a polar crystal structure. In contrast, the $n \geq 4$ phases are nonpolar structures.[28] However, the n = 2 structures are widely reported to exhibit multiferroic properties, while their average crystal structure based on neutron and X-ray diffraction belongs to the centrosymmetric $P4/mmm$ space group. More careful studies have revealed further symmetry breaking in these structures.[29−31] Distinct octahedral tilting, metal off-centering, and intralayer polarization switching were inferred for the n = 2 and 3 phases from the second-harmonic-generation (SHG) studies. Notwithstanding such ambiguity, the observation of multiferroic properties inspired us to investigate their unexplored piezocatalytic properties when n = 2. The n = 2 phase of the $Sr_2Bi_3Nb_2O_{11}Br$ crystal in the $P4/mmm$ space group is shown in Figure 1a−c. Structurally, it comprises four distinct lattice oxygen sites. O1 and O2 belong to the 12-coordinated Bi-alone site, where the polyhedron distortion, as confirmed in the n = 1 phase, is expected to be influenced by the presence of stereochemically active Bi $6s^2$ lone pairs and the off-centering of adjacent metal octahedra due to the second-order Jahn−Teller effect (Figure 1d). O3 and O4 are situated at the interface of $[BiSrO_2]^+$ and the perovskite layers and near the halide layer, respectively. The presence of the Bi_2O_2 layer and the distortion-induced structure of $Sr_2Bi_3Nb_2O_{11}Br$ as revealed by the SHG studies is likely to confer inherent polarization properties, contributing to efficient and fatigue-resistant piezocatalytic activity.[28,29,32−34]

The SA phase of $Sr_2Bi_3Nb_2O_{11}Br$, featuring double perovskite layers, was synthesized using a molten flux method, employing a eutectic mixture of NaBr and KBr as flux at 800 °C for 4 h. The purity and crystallinity of the product were assessed using powder X-ray diffraction (XRD, as shown in Figure 2a). All diffraction peaks could be attributed to pure $Sr_2Bi_3Nb_2O_{11}Br$ with lattice constants of a = 3.9231 Å, b = 3.9231 Å, and c = 18.6066 Å, confirming its purity.[24]

To evaluate the morphology of the as-synthesized $Sr_2Bi_3Nb_2O_{11}Br$, scanning electron microscopy (SEM, Figures 2b and S1) and transmission electron microscopy (TEM
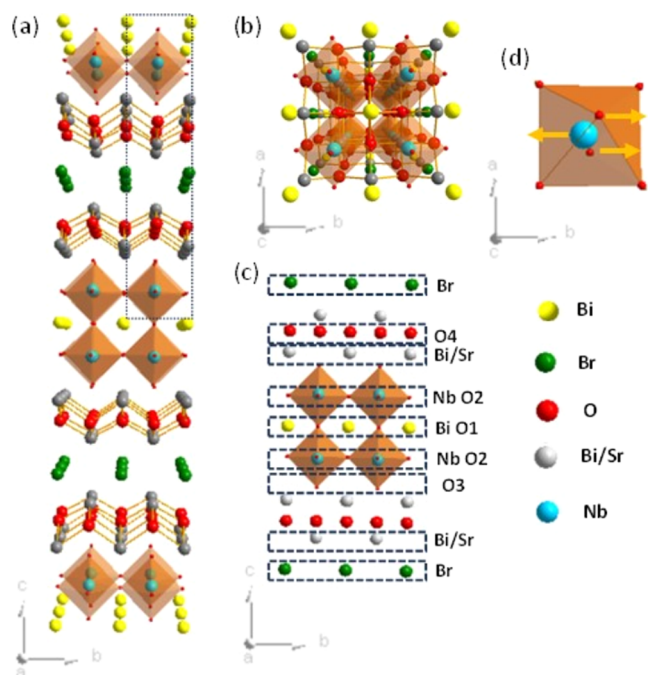
Figure 1. Crystal structure of $Sr_2Bi_3Nb_2O_{11}Br$ observed along two different planes: (a) *bc* plane and (b) *ab* plane. (c) Various lattice oxygen configurations within $Sr_2Bi_3Nb_2O_{11}Br$. (d) The perovskite block indicates the octahedral off-centering of Nb.

Figure 2c) were employed. These analyses revealed that the sample consists of rectangular nanoplates with an approximate edge length of 2−10 μm. Subsequently, atomic force microscopy (AFM, Figure 2d) confirmed the nanoplate morphology, indicating a thickness of ∼90 (±30) nm and smooth surfaces. These nanoplates exhibit a surface area of 7.9 ± 1.5 m^2/g (Figure S2). High-resolution TEM (HRTEM) and selected area electron diffraction (SAED) analyses revealed that the nanoplates are single crystalline. The HRTEM images of the nanoplate displayed in Figure 2e,f contain lattice fringes of 0.39 and 0.28 nm corresponding to the (110) and (020) planes, respectively, suggesting that the basal facet of the nanoplates is {001}.[7,35] A typical SAED pattern of a nanoplate (Figure 2g) recorded along the [001] zone axis confirms the dominant exposure of {001} facets and the single-crystalline nature of $Sr_2Bi_3Nb_2O_{11}Br$ nanoplates. It may be noted that the flux method appears advantageous, unlike the traditional solid-state synthesis method that requires multiple heating and grinding steps and a much longer annealing times. Besides, the traditional particles may be deemed unsuitable for piezocatalysis due to a smaller surface area and the polycrystalline nature that can temper with pressure transmission.

X-ray photoelectron spectroscopy (XPS) was employed to analyze the elemental composition and oxidation states. The survey spectrum (Figure S3a) confirmed the presence of all four elements. The high-resolution Bi 4f spectrum (Figure 2h) can be deconvoluted into four distinct peaks. Among these, the peaks at 159.4 and 164.6 eV correspond to Bi $4f_{7/2}$ and Bi $4f_{5/2}$, respectively, indicating Bi^{3+} ions, while the low-intensity peaks at 158.58 and 164.01 eV were attributed to a lower valence state of Bi^{2+}.[36] The presence of a tiny amount of Bi^{2+} suggests the reduction of Bi^{3+} to Bi^{2+} during synthesis, resulting in oxygen vacancies to maintain charge neutrality.[37] High-resolution O 1s spectrum (Figure 2i) contains peaks at 529.8 and 531.3 eV, representing lattice oxygen and oxygen

vacancies, respectively, confirming the presence of a small number of oxygen vacancies to accommodate Bi^{2+}.[38] On the other hand, the high-resolution Nb 3d and Sr 3d spectra (Figure S3b,c) did not show any lower valence peaks, suggesting a minimal probability of oxygen vacancy formation in perovskite layers due to the stronger (Sr/Nb)−O bonds compared to Bi−O.[39,40] The high-resolution Br 3d spectrum (Figure S3d) was deconvoluted into two peaks corresponding to $3d_{5/2}$ and $3d_{3/2}$, confirming the presence of Br. These $Sr_2Bi_3Nb_2O_{11}Br$ nanoplates have an average optical band gap of 2.58 eV (Figure S4).[24] Additionally, the TEM energy-dispersive spectroscopy (EDS) elemental mapping also confirms the presence of all of the constituent elements in the $Sr_2Bi_3Nb_2O_{11}Br$ nanoplates (Figure S5).

Piezoelectric force microscopy (PFM) analysis was conducted to investigate the piezoelectric properties of the nanoplate. This involved applying an alternating current (AC) voltage for mapping alongside a sweeping direct current (DC) voltage to the scanning tip for estimating voltage-induced distortion in the nanoplate. Figure 3a,b illustrates the corresponding phase and amplitude images of a single nanoplate. Local piezoresponse hysteresis loops (Figure 3c) were generated by sweeping the DC bias from −10 to 10 V, which produced a distinctive butterfly-shaped amplitude loop characteristic of piezoelectric materials corresponding to a piezoelectric coefficient of 244 pm/V. The phase-angle−voltage hysteresis plot (Figure 3d) exhibited a 180° shift upon DC bias reversal, confirming polarization switching within the nanoplate.

To measure the piezopotential on the nanoplate surface, a piezoelectric potential map (Figure 3e,f) was generated by scanning a Kelvin probe force microscopy (KPFM) cantilever over the nanoplate, revealing a surface potential of 410 mV. The work function (φ) was determined using the equation[8,41]

$$\varphi_{tip} - \varphi_{sample} = V_{CPD}/e$$

where V_{CPD} is the contact potential difference between the tip and the nanoplate, φ_{tip} and φ_{sample} represent the work functions of the tip and sample, respectively, and e is the elementary charge. The work function of the nanoplate was estimated as 4.47 eV, with highly oriented pyrolytic graphite (HOPG, φ = 4.66 eV), serving as a reference for calibrating φ_{tip}, which is superior to n = 1, Bi_4TaO_8Cl to suggest facile charge transfer during catalysis.[7]

■ PIEZOCATALYTIC WATER SPLITTING

Motivated by the high surface area, single-crystalline nature, and prominent piezoelectric properties, we investigated the piezocatalytic efficiencies of the $Sr_2Bi_3Nb_2O_{11}Br$ nanoplatelets toward pure water splitting experiments under ultrasonic conditions to produce hydrogen. We further used 10 vol % ethanol as a hole scavenger but no expensive cocatalyst such as Pt as in photocatalysis. As seen in Figure 4a, the nanoplates exhibit excellent performance with consistent production of H_2 for 4 h while using an ultrasonic frequency of 37 kHz, corresponding to a production rate of ∼5.3 mmol/h/g (significantly higher than that without ethanol as expected, as shown in Figure S6). The H_2 production activity of the nanoplates was found to vary under different powers and frequencies of ultrasonication. Figure 4b shows the influence of two different ultrasonic frequencies on the production rate. While 80 kHz frequency also gave a consistent H_2 production
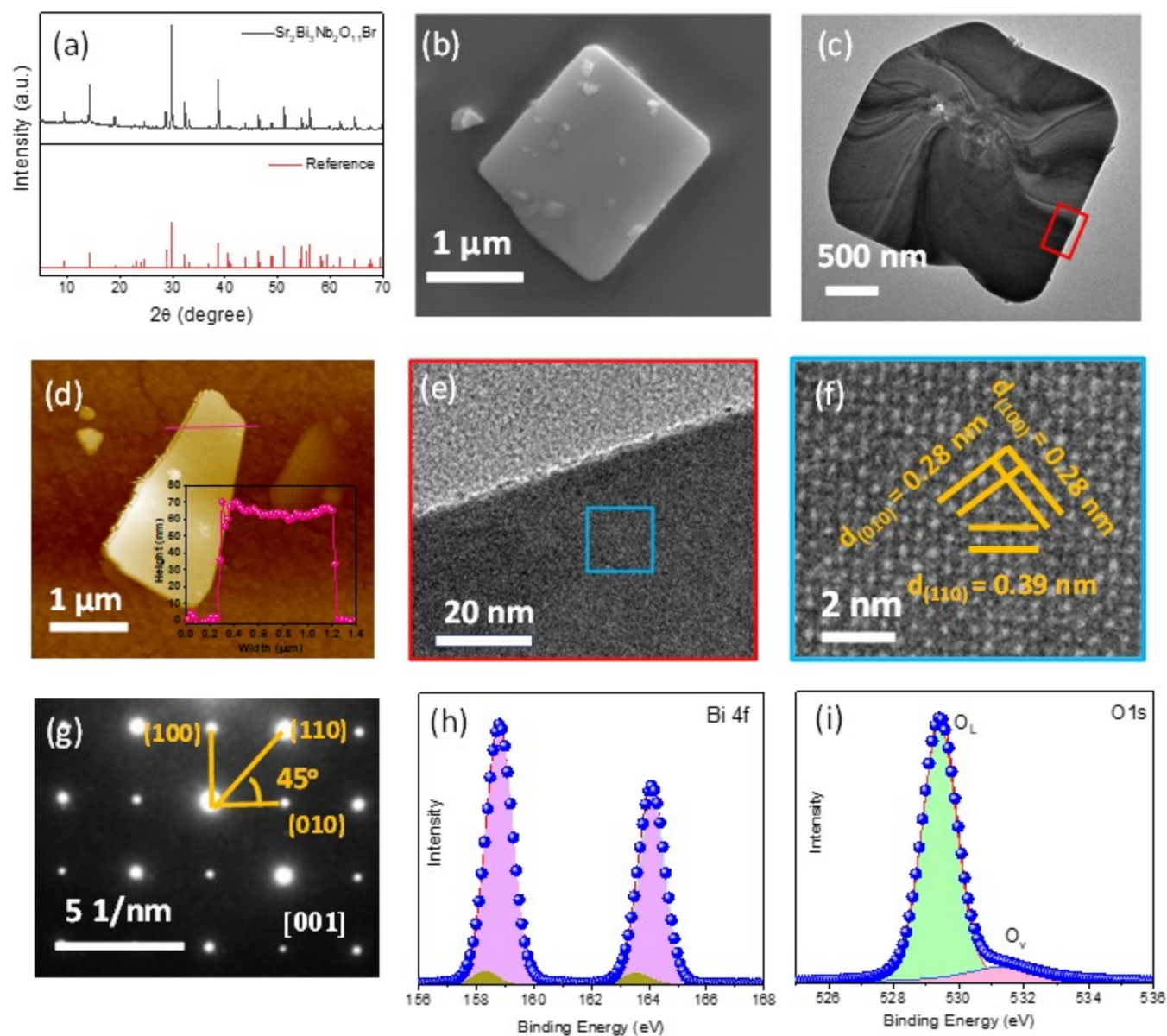
Figure 2. (a) Powder XRD pattern of $Sr_2Bi_3Nb_2O_{11}Br$, field emission, (b) SEM, (c) TEM images, and (d) atomic force microscopy image and the corresponding height profile (inset, ~70 nm) confirms the formation of the $Sr_2Bi_3Nb_2O_{11}Br$ nanoplates. (e, f) HRTEM images and (g) single-crystalline SAED pattern acquired on a single nanoplate. (h, i) High-resolution Bi 4f and O 1s XPS spectra of the sample.

at a rate ~1.2 mmol/h/g, the higher activity achieved at 37 kHz is probably due to proximity to the resonance frequency of the catalyst.[11] Moreover, the H_2 generation rate monotonously increased from 2.5 to 2.88, 4, and 5.3 mmol/h/g when the ultrasonic power (at 37 kHz) was increased from 40 to 60, 80, and 100%, respectively (Figure 4c). The higher vibrational power could lead to higher stress (T) and more piezoelectric charge density (Q_p) on the catalyst's surface, resulting in higher catalytic efficiency, following the relationship $Q_p = dT$, (d is the piezoelectric coefficient of the nanoplates).

We further investigated the piezocatalytic seawater splitting efficiency of the nanoplates using 3% NaCl solutions (weight/volume) and real seawater to investigate the effect of salts and other impurities on H_2 production. As seen in Figure 4d, the production rate slightly decreased to 4.1 mmol/h/g in the NaCl solution, and the same was 3.5 mmol/h/g when using water from the Bay of Bengal. The decreases in catalytic

activities in seawater splitting can be attributed to the blocking of active sites and also the presence of cations in saline water that are known to undergo either electrodeposition under reductive conditions to decrease faradic efficiency or as hydroxides.[7,9]

The H_2 production rate of ~5.3 mmol/h/g in pure water is significantly higher than those achieved previously by using other piezocatalysts, such as $BaTiO_3$, $SrTiO_3$, Bi_4TaO_8Cl, etc., as seen from a detailed comparison in Table S1. In addition, although we observed a slight (~22%) decrease in H_2 production in seawater compared to pure water, this rate remains notably superior to those achieved via photocatalytic means using cocatalyst-loaded Sillen−Aurivillius phases, other oxide photocatalysts (Figure 4e), as well as previously reported piezocatalysts (Figure 4f and Table S1). For example, a ~60% decrease to 0.05 mmol/h/g was observed while using a traditional $BaTiO_3$ piezocatalyst.[42] Similarly, in the case of the
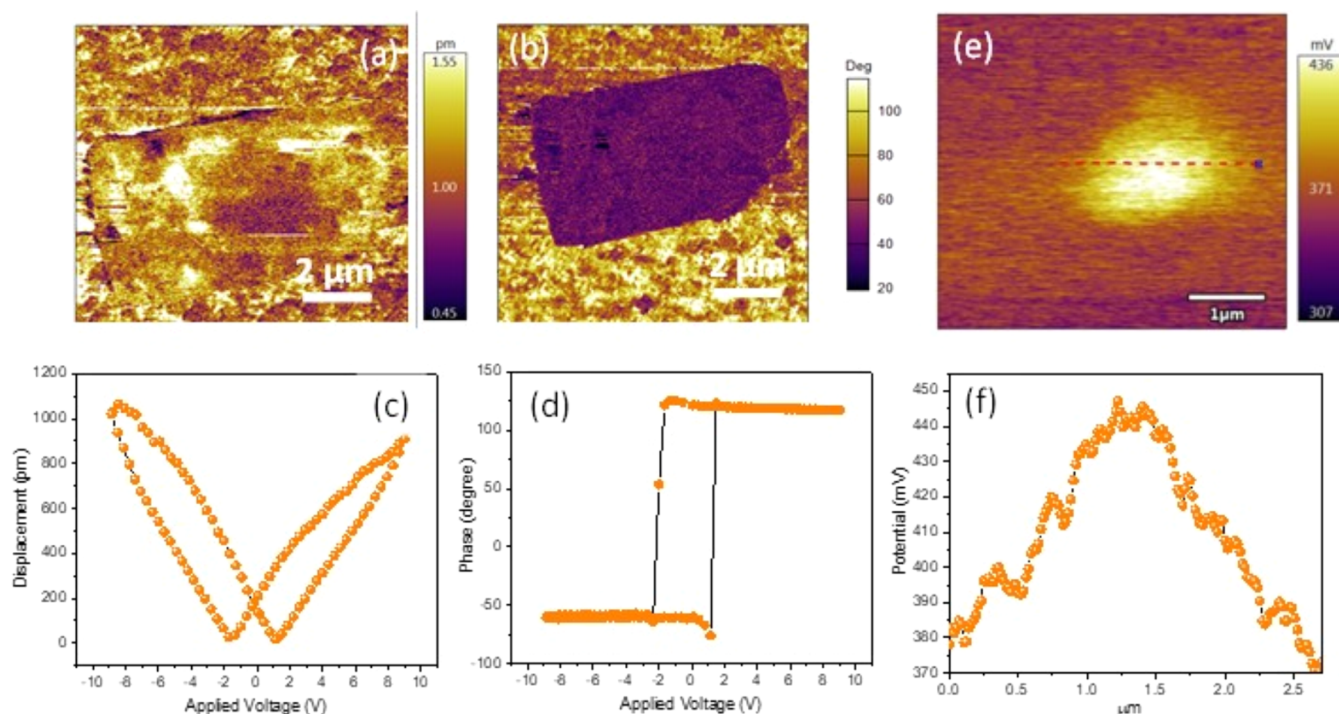
Figure 3. (a, b) Amplitude and phase images of a $Sr_2Bi_3Nb_2O_{11}Br$ nanoplate and their corresponding (c) displacement−voltage and (d) phase curves, respectively. (e) KPFM potential mapping image of the plate and the corresponding (f) surface potential.

single-perovskite SA phase of Bi_4TaO_8Cl, a marked decrease of ~40% to 0.85 mmol/h/g was reported.[7]

The underlying principle driving the piezocatalytic hydrogen generation using $Sr_2Bi_3Nb_2O_{11}Br$ nanoplates is illustrated in Figure 4g. When these nanoplates are subjected to ultra-sonication, the implosive collapse of a cavitation bubble formed during piezocatalysis exerts mechanical pressure on them.[8] This pressure triggers a piezoelectric effect, leading to the generation of positive and negative charges on the nanoplatelet surfaces. The negative charges (q^-) attract protons in water, promoting H_2 production. Simultaneously, the positive charges (q^+) on the opposite side of the nanoplatelets are neutralized by the sacrificial agent.[11]

LONG-TERM STABILITY OF THE SILLEN−AURIVILLIUS PHASES

Considering that the past studies have been focused on developing highly efficient piezocatalysts but their stability being checked for barely 10−15 h, while the long-term stability evaluation is critical for sustainability, the $Sr_2Bi_3Nb_2O_{11}Br$ nanoplates were subjected to use for 152 h of piezocatalytic hydrogen production, with the evacuation of the reaction system at 4 h intervals. We anticipated high stability due to the presence of the $(Bi_2O_2)^{2+}$ layers in its crystal structure, as discussed before, which should help retain the crystallinity and morphology of the nanoplates. Notably, as depicted in Figures 5 and S7, there was a minimal alteration in hydrogen production even after 152 h of ultrasonic irradiation, demonstrating significant stability of the nanoplates under ultrasonic conditions and retention of the piezocatalytic properties. A range of analyses were performed to evaluate the used nanoplates. Initially, XRD affirmed the catalyst's stability at the bulk level (Figure S8). Subsequent examinations of morphology using SEM (Figure S9a,b), TEM (Figure S9c), and AFM (Figure S10) revealed no noticeable changes in

nanoplate morphology. Additionally, Brunauer−Emmett−Teller (BET, Figure S11) data also indicated negligible alterations in the surface area. The surface of the used catalyst was further characterized by X-ray absorption spectroscopy (Figure S12) and does not show any remarkable change, further confirming stability.

The piezoelectric properties of the used $Sr_2Bi_3Nb_2O_{11}Br$ nanoplates were also assessed via piezoelectric force microscopy. Figure 6a,b illustrates the typical amplitude and phase image of a used nanoplate, with corresponding spectroscopic data shown in Figure 6c,d. The discernible butterfly loop in the displacement versus potential plot (Figure 6c) demonstrates that the $Sr_2Bi_3Nb_2O_{11}Br$ nanoplates remain piezoelectric after catalysis with a piezoelectric coefficient of d_{33} = 105 pm/V. The corresponding phase-angle−voltage hysteresis plot (Figure 6d) shows a 180° shift under the reversal of the DC bias and confirms the retained polarization switching within the nanoplate. The open-circuit potential (V_p) was also calculated to find out the magnitude of band bending by following the equation[8]

$$V_p = \frac{W_3 T_3 d_{33}}{e_o e_r}$$

where W_3 is the thickness of the nanoplate, T_3 is the applied pressure, d_{33} is the piezoelectric coefficient, e_o is the permittivity of free space, and e_r is the relative permittivity. Here, the thickness of the nanoplate and the piezoelectric coefficient are ~70 nm and 105 pm/V, respectively, while e_r has been considered as 150.[43] However, the actual pressure generated under sonication is rather vaguely reported in the literature in the range of 0.1 to 10 GPa for a single cavitation bubble collapse. If we consider an average T_3 = 1 GPa, the calculated open-circuit voltage across the used $Sr_2Bi_3Nb_2O_{11}Br$ nanoplate is ~5.5 V and so is the band-bending potential. Mott−Schottky measurements on the nanoplates show

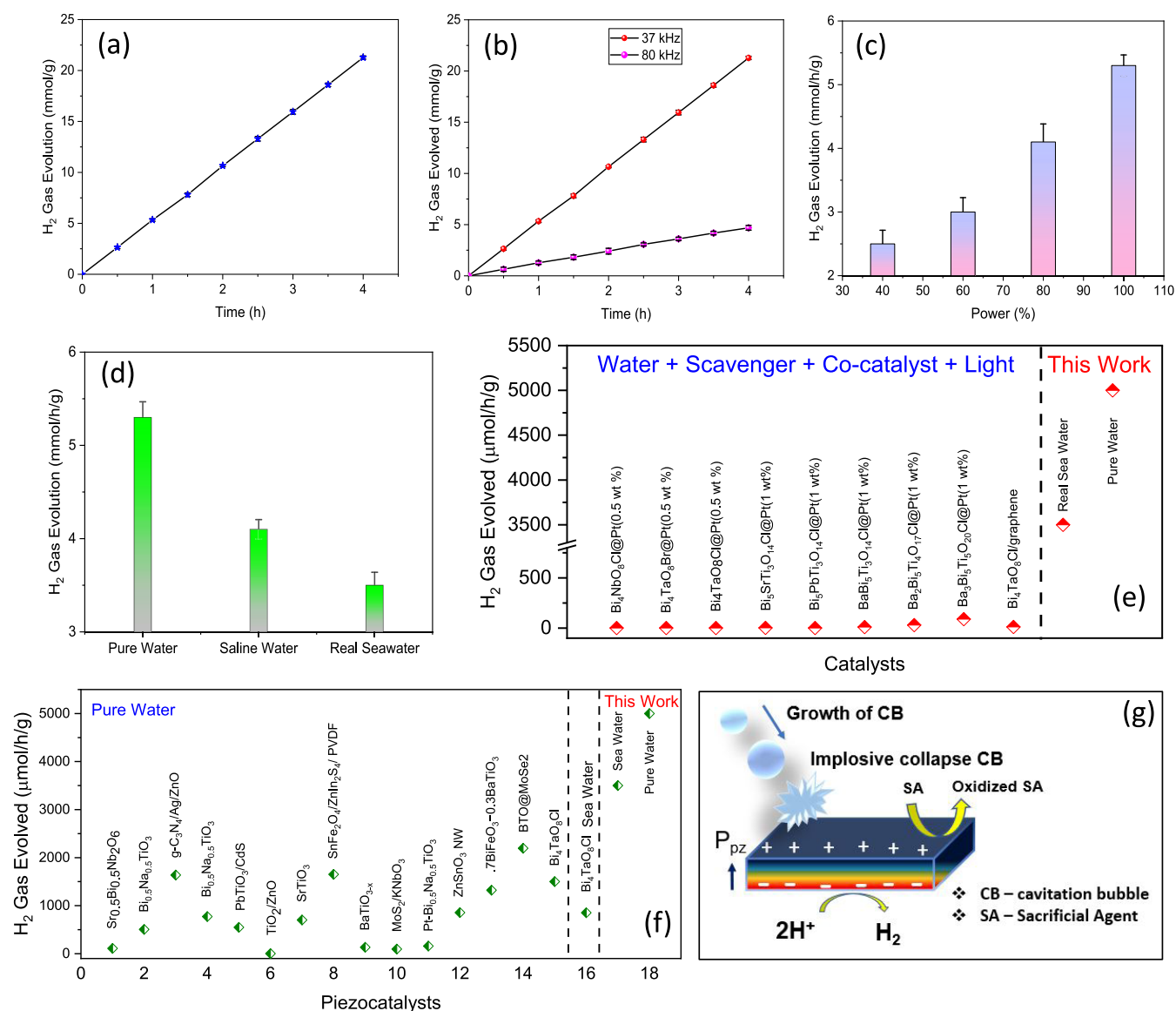**Figure 4.** (a) Plot showing the rate of H_2 production under ultrasound exposure by the $Sr_2Bi_3Nb_2O_{11}Br$ nanoplates. (b, c) H_2 production efficiencies of the nanoplates as a function of ultrasonic frequency and power, respectively. (d) Comparison of H_2 production from NaCl solution, pure and real seawater. Comparison of the current H_2 production performances in pure water and seawater with those observed in past studies using (e) photocatalytic approach from Pt-loaded SA phases, as well as (f) other piezocatalysts reported in the literature (Table S1 in the Supporting Information includes the detailed reaction conditions). (g) Schematic showing H_2 production over $Sr_2Bi_3Nb_2O_{11}Br$ nanoplates under piezocatalytic conditions.

conduction and valence band positions of (-0.5 ± 0.09) and (2.16 ± 0.09) V vs RHE, respectively. Considering that only valence band electrons participate in piezocatalysis and hydrogen reduction potential of 0 V vs RHE, a band bending of only ~2.16 eV is required for the $Sr_2Bi_3Nb_2O_{11}Br$ nanoplates for efficient hydrogen generation, much lower than 5.5 V, leading to a fatigue-free, consistent production over 150 h.

CONCLUSIONS

In conclusion, we introduce a novel, flux-based method to produce the $n = 2$ Sillen−Aurivillius phase of $Sr_2Bi_3Nb_2O_{11}Br$ in a nanoplate morphology with precise control over facets, leading to a high surface area, single crystallinity, pronounced piezoelectric properties, and enhanced piezocatalytic activity. These nanoplates demonstrate exceptionally high efficiency in

splitting water and producing hydrogen without the need for additional cocatalysts, achieving a rate of 5.3 mmol/g/h. We also extend their application to seawater splitting, achieving a rate of 4.1 and 3.5 mmol/g/h for simulated and real seawater that even surpasses the existing metal-based piezo- and photocatalysts used in pure water. We further establish the "fatigue-free" piezocatalytic activity of the nanoplates for the first time by subjecting them to over 150 h of continuous stress (an order of magnitude higher than before) but with negligible loss in hydrogen production activity.

METHODS

Flux Synthesis of $Sr_2Bi_3Nb_2O_{11}Br$. $Sr_2Bi_3Nb_2O_{11}Br$ nanoplates were synthesized by mixing a stoichiometric molar ratio (2:1:1:1) of $SrCO_3$, Bi_2O_3, Nb_2O_5, and BiOBr as starting materials. A molten salt consisting of a eutectic mixture of KCl and NaCl (1:1) was employed as a flux to promote the reaction and ensure the formation of the
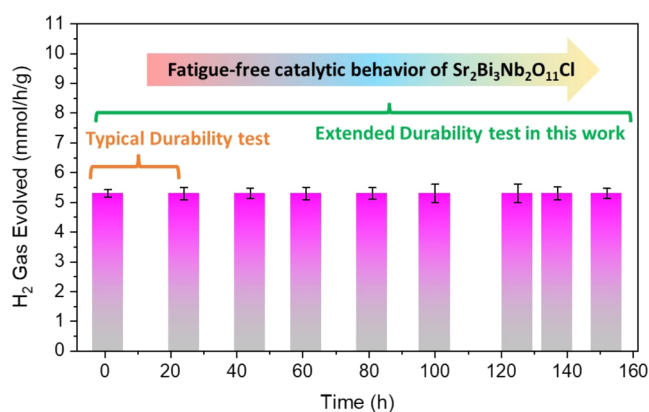
Figure 5. Plot showing sustained piezocatalytic H_2 production by $Sr_2Bi_3Nb_2O_{11}Br$ nanoplates for over 152 h.

nanoplates. The solute concentration of the flux was maintained at 3.2 mol % relative to the total amount of $Sr_2Bi_3Nb_2O_{11}Br$ and flux. The precursors and flux were thoroughly ground with a mortar and pestle, placed in an aluminum crucible, and then heated at 1073 K for 4 h in a muffle furnace. Following natural cooling, the resulting product underwent washing with deionized water and filtration, and the obtained off-white powder was dried at room temperature.

Piezocatalytic Hydrogen Evolution Experiments. Piezocatalytic hydrogen evolution experiments were performed by dispersing 5 mg of $Sr_2Bi_3Nb_2O_{11}Br$ nanoplates in a 10 volume percent ethanolic aqueous solution of 30 mL volume, and the resulting solution was enclosed in a 500 mL round-bottom flask (RB). To eliminate air, the system underwent a 1 h purge with nitrogen (N_2). Following this, the RB was immersed in an ultrasonic bath (ELMA Elmasonic P300H, 110 W power) with switchable frequencies of 37 and 80 kHz. The temperature of the piezocatalytic system was kept constant at 30 °C

using a water-cooling system. Gas generated during the experiments was intermittently extracted with a gastight syringe and subjected to analysis through gas chromatography (GC). For seawater-splitting experiments, seawater was collected from a rocky beach in Pondicherry, India, situated on the Bay of Bengal, and was used after sedimentation.

ASSOCIATED CONTENT

Supporting Information

The Supporting Information is available free of charge at https://pubs.acs.org/doi/10.1021/acs.chemmater.4c00828.

Additional X-ray diffraction, SEM, BET, XPS, diffuse reflectance spectroscopy (DRS), AFM, comparison table, and experimental details (PDF)

AUTHOR INFORMATION

Corresponding Author

Ujjal K. Gautam − *Department of Chemical Sciences, Indian Institute of Science Education and Research (IISER)-Mohali, Mohali, S.A.S. Nagar, Punjab 140306, India;* orcid.org/0000-0002-0731-0429; Email: ujjalgautam@iisermohali.ac.in, ujjalgautam@gmail.com

Authors

Maqsuma Banoo − *Department of Chemical Sciences, Indian Institute of Science Education and Research (IISER)-Mohali, Mohali, S.A.S. Nagar, Punjab 140306, India*

Arjun Kumar Sah − *Department of Chemical Sciences, Indian Institute of Science Education and Research (IISER)-Mohali, Mohali, S.A.S. Nagar, Punjab 140306, India*

Figure 6. (a, b) Amplitude and phase images of a used $Sr_2Bi_3Nb_2O_{11}Br$ nanoplate and their corresponding (c) displacement−voltage curve and (d) phase curve, respectively.

Raj Sekhar Roy − *Department of Chemical Sciences, Indian Institute of Science Education and Research (IISER)-Mohali, Mohali, S.A.S. Nagar, Punjab 140306, India*
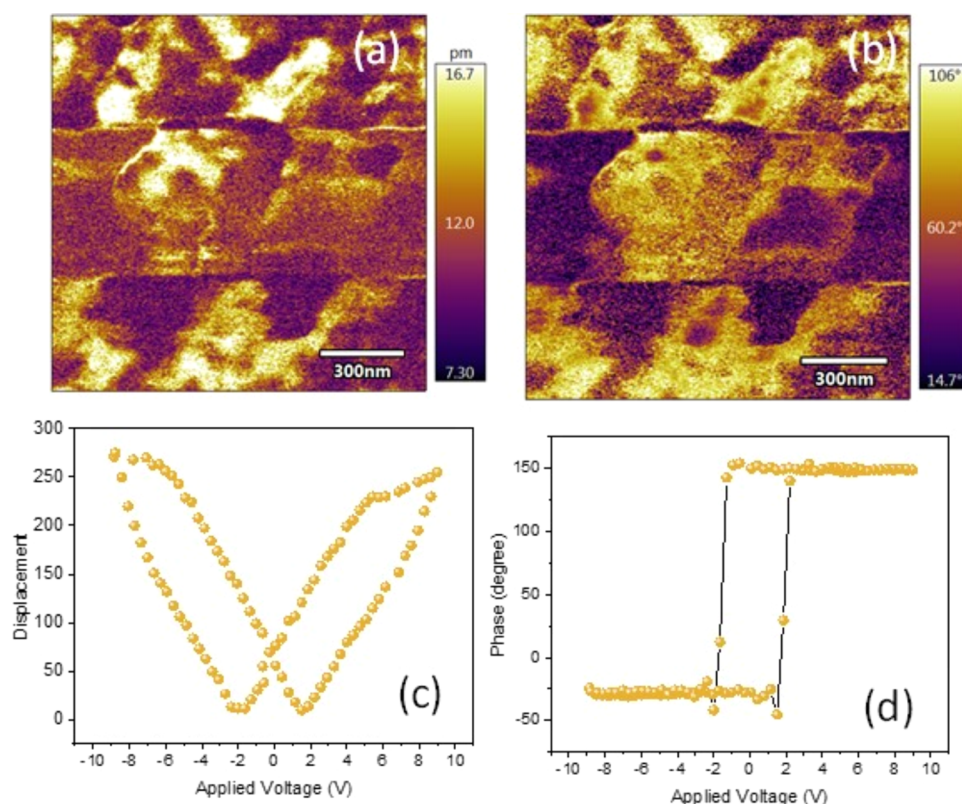
Pooja Bhardwaj − *Department of Physical Sciences, Indian Institute of Science Education and Research (IISER)-Mohali, Mohali, S.A.S. Nagar, Punjab 140306, India*

Digamber G. Porob − *School of Chemical Sciences, Goa University, Taleigao Plateau, Goa 403206, India*

Goutam Sheet − *Department of Physical Sciences, Indian Institute of Science Education and Research (IISER)-Mohali, Mohali, S.A.S. Nagar, Punjab 140306, India;* ⊚ orcid.org/0000-0002-5290-1738

Complete contact information is available at:
https://pubs.acs.org/10.1021/acs.chemmater.4c00828

Author Contributions

‖M.B. and A.K.S. contributed equally to this work.

Notes

The authors declare no competing financial interest.

◼ REFERENCES

(1) Suzuki, H.; Ozaki, D.; Ishii, Y.; Tomita, O.; Kato, D.; Nozawa, S.; Nakashima, K.; Saeki, A.; Kageyama, H.; Abe, R. A Sillén Oxyhalide SrBi3O4Cl3 as a Promising Photocatalyst for Water Splitting: Impact of the Asymmetric Structure on Light Absorption and Charge Carrier Dynamics. *J. Mater. Chem. A* **2023**, *11* (28), 15159−15167.

(2) Lin, L.; Ma, Y.; Vequizo, J. J. M.; Nakabayashi, M.; Gu, C.; Tao, X.; Yoshida, H.; Pihosh, Y.; Nishina, Y.; Yamakata, A.; Shibata, N.; Hisatomi, T.; Takata, T.; Domen, K. Efficient and Stable Visible-Light-Driven Z-Scheme Overall Water Splitting Using an Oxysulfide H2 Evolution Photocatalyst. *Nat. Commun.* **2024**, *15* (1), No. 397.

(3) Xiao, S. T.; Yin, R.; Wu, L.; Wu, S. M.; Tian, G.; Shalom, M.; Wang, L. Y.; Wang, Y. T.; Pu, F. F.; Barad, H. N.; Wang, F.; Yang, X. Y. Hierarchically Porous Few-Layer Carbon Nitride and Its High H+Selectivity for Efficient Photocatalytic Seawater Splitting. *Nano Lett.* **2023**, *23* (10), 4390−4398.

(4) Roy, R. S.; Mondal, S.; Mishra, S.; Banoo, M.; Sahoo, L.; Kumar, A.; Vinod, C. P.; De, A. K.; Gautam, U. K. Covalently Interconnected Layers in G-C3N4: Toward High Mechanical Stability, Catalytic Efficiency and Sustainability. *Appl. Catal., B* **2023**, *322*, 122069.

(5) Su, R.; Wang, Z.; Zhu, L.; Pan, Y.; Zhang, D.; Wen, H.; Luo, Z. D.; Li, L.; Li, F.-t.; Wu, M.; He, L.; Sharma, P.; Seidel, J. Strain-Engineered Nano-Ferroelectrics for High-Efficiency Piezocatalytic Overall Water Splitting. *Angew. Chem., Int. Ed.* **2021**, *60* (29), 16019−16026.

(6) Su, R.; Hsain, H. A.; Wu, M.; Zhang, D.; Hu, X.; Wang, Z.; Wang, X.; Li, F.-t.; Chen, X.; Zhu, L.; Yang, Y.; Yang, Y.; Lou, X.; Pennycook, S. J. Nano-Ferroelectric for High Efficiency Overall Water Splitting under Ultrasonic Vibration. *Angew. Chem., Int. Ed.* **2019**, *58* (42), 15076−15081.

(7) Banoo, M.; Roy, R. S.; Bhakar, M.; Kaur, J.; Jaiswal, A.; Sheet, G.; Gautam, U. K. Bi4TaO8Cl as a New Class of Layered Perovskite Oxyhalide Materials for Piezopotential Driven Efficient Seawater Splitting. *Nano Lett.* **2022**, *22* (22), 8867−8874.

(8) Banoo, M.; Kaur, J.; Sah, A. K.; Roy, R. S.; Bhakar, M.; Kommula, B.; Sheet, G.; Gautam, U. K. Universal Piezo-Photocatalytic Wastewater Treatment on Realistic Pollutant Feedstocks by Bi4TaO8Cl: Origin of High Efficiency and Adjustable Synergy. *ACS Appl. Mater. Interfaces* **2023**, *15* (27), 32425−32435.

(9) Starr, M. B.; Wang, X. Fundamental Analysis of Piezocatalysis Process on the Surfaces of Strained Piezoelectric Materials. *Sci. Rep.* **2013**, *3* (1), No. 2160.

(10) Wang, K.; Han, C.; Li, J.; Qiu, J.; Sunarso, J.; Liu, S. The Mechanism of Piezocatalysis: Energy Band Theory or Screening Charge Effect? *Angew. Chem., Int. Ed.* **2022**, *61* (6), No. e202110429.

(11) You, H.; Wu, Z.; Zhang, L.; Ying, Y.; Liu, Y.; Fei, L.; Chen, X.; Jia, Y.; Wang, Y.; Wang, F.; Ju, S.; Qiao, J.; Lam, C. H.; Huang, H. Harvesting the Vibration Energy of BiFeO3 Nanosheets for Hydrogen Evolution. *Angew. Chem., Int. Ed.* **2019**, *58* (34), 11779−11784.

(12) Li, H.; Tian, C.; Deng, Z. D. Energy Harvesting from Low-Frequency Applications Using Piezoelectric Materials. *Appl. Phys. Rev.* **2014**, *1* (4), No. 041301.

(13) Ghemari, Z.; Belkhiri, S.; Saad, S. A Piezoelectric Sensor with High Accuracy and Reduced Measurement Error. *J. Comput. Electron.* **2024**, *23*, No. 0123456789.

(14) Hong, K. S.; Xu, H.; Konishi, H.; Li, X. Direct Water Splitting through Vibrating Piezoelectric Microfibers in Water. *J. Phys. Chem. Lett.* **2010**, *1* (6), 997−1002.

(15) Hu, C.; Chen, F.; Wang, Y.; Tian, N.; Ma, T.; Zhang, Y.; Huang, H. Exceptional Cocatalyst-Free Photo-Enhanced Piezocatalytic Hydrogen Evolution of Carbon Nitride Nanosheets from Strong In-Plane Polarization. *Adv. Mater.* **2021**, *33* (24), No. 2101751.

(16) Zhou, X.; Yan, F.; Wu, S.; Shen, B.; Zeng, H.; Zhai, J. Remarkable Piezophoto Coupling Catalysis Behavior of BiOX/BaTiO3 (X = Cl, Br, Cl0.166Br0.834) Piezoelectric Composites. *Small* **2020**, *16* (26), No. 2001573.

(17) Ohno, T.; Bai, L.; Hisatomi, T.; Maeda, K.; Domen, K. Photocatalytic Water Splitting Using Modified GaN:ZnO Solid Solution under Visible Light: Long-Time Operation and Regeneration of Activity. *J. Am. Chem. Soc.* **2012**, *134* (19), 8254−8259.

(18) Fang, Y.; Wei, C.; Bian, Z.; Yin, X.; Liu, B.; Liu, Z.; Chi, P.; Xiao, J.; Song, W.; Niu, S.; Tang, C.; Liu, J.; Ge, X.; Xu, T.; Wang, G. Unveiling the Nature of Pt-Induced Anti-Deactivation of Ru for Alkaline Hydrogen Oxidation Reaction. *Nat. Commun.* **2024**, *15* (1), No. 1614.

(19) Li, F. M.; Huang, L.; Zaman, S.; Guo, W.; Liu, H.; Guo, X.; Xia, B. Y. Corrosion Chemistry of Electrocatalysts. *Adv. Mater.* **2022**, *34* (52), No. 2200840.

(20) Zhang, X.; Bo, C.; Cao, S.; Cheng, Z.; Xiao, Z.; Liu, X.; Tan, T.; Piao, L. Stability Improvement of a Pt/TiO2 Photocatalyst during Photocatalytic Pure Water Splitting. *J. Mater. Chem. A* **2022**, *10* (45), 24381−24387.

(21) Park, B. H.; Kang, B. S.; Bu, S. D.; Noh, T. W.; Lee, J.; Jo, W. Lanthanum-substituted bismuth titanate for use in non-volatile memories44352. *Nature* **1999**, *401*, 682−684.

(22) Pan, Z.; Wang, P.; Hou, X.; Yao, L.; Zhang, G.; Wang, J.; Liu, J.; Shen, M.; Zhang, Y.; Jiang, S.; Zhai, J.; Wang, Q. Fatigue-Free Aurivillius Phase Ferroelectric Thin Films with Ultrahigh Energy Storage Performance. *Adv. Energy Mater.* **2020**, *10* (31), No. 2001536.

(23) Yao, Y.; Peng, Y.; Li, L.; Zhang, X.; Liu, X.; Hong, M.; Luo, J. Exploring a Fatigue-Free Layered Hybrid Perovskite Ferroelectric for Photovoltaic Non-Volatile Memories. *Angew. Chem., Int. Ed.* **2021**, *60* (19), 10598−10602.

(24) Nakada, A.; Saeki, A.; Higashi, M.; Kageyama, H.; Abe, R. Two-Step Synthesis of Sillén-Aurivillius Type Oxychlorides to Enhance Their Photocatalytic Activity for Visible-Light-Induced Water Splitting. *J. Mater. Chem. A* **2018**, *6* (23), 10909−10917.

(25) Nakada, A.; Higashi, M.; Kimura, T.; Suzuki, H.; Kato, D.; Okajima, H.; Yamamoto, T.; Saeki, A.; Kageyama, H.; Abe, R. Band Engineering of Double-Layered Sillén-Aurivillius Perovskite Oxychlorides for Visible-Light-Driven Water Splitting. *Chem. Mater.* **2019**, *31* (9), 3419−3429.

(26) Banoo, M.; Chatterjee, K.; Mondal, S.; Vinod, C. P.; Gautam, U. K. A 'Self-Activating' Bi3TaO7-Bi4TaO8Br Photocatalyst and Its Use in the Sustainable Production of pro-Fluorophoric Rhodamine-110. *Green Chem.* **2022**, *24* (14), 5514−5523.

(27) Chatterjee, K.; Banoo, M.; Mondal, S.; Sahoo, L.; Gautam, U. K. Synthesis of Bi3TaO7-Bi4TaO8Br Composites in Ambient Air and

Their High Photocatalytic Activity upon Metal Loading. *Dalton Trans.* **2019**, *48* (21), 7110−7116.

(28) Zhong, C.; Ishii, Y.; Tassel, C.; Zhu, T.; Kato, D.; Kurushima, K.; Fujibayashi, Y.; Saito, T.; Ogawa, T.; Kuwabara, A.; Mori, S.; Kageyama, H. Lone-Pair-Induced Intra- and Interlayer Polarizations in Sillén-Aurivillius Layered Perovskite Bi4NbO8Br. *Inorg. Chem.* **2022**, *61* (25), 9816−9822.

(29) Kusainova, A. M.; Lightfoot, P.; Zhou, W.; Stefanovich, S. Y.; Mosunov, A. V.; Dolgikh, V. A. Ferroelectric Properties and Crystal Structure of the Layered Intergrowth Phase Bi3Pb2Nb2O11Cl. *Chem. Mater.* **2001**, *13* (12), 4731−4737.

(30) Liu, S.; Blanchard, P. E. R.; Avdeev, M.; Kennedy, B. J.; Ling, C. D. Designing New n = 2 Sillen-Aurivillius Phases by Lattice-Matched Substitutions in the Halide and [Bi2O2]2+ Layers. *J. Solid State Chem.* **2013**, *205*, 165−170.

(31) Liu, S.; Miiller, W.; Liu, Y.; Avdeev, M.; Ling, C. D. Sillen-Aurivillius Intergrowth Phases as Templates for Naturally Layered Multiferroics. *Chem. Mater.* **2012**, *24* (20), 3932−3942.

(32) Bersuker, I. B.; Polinger, V. Perovskite Crystals: Unique Pseudo-Jahn−Teller Origin of Ferroelectricity, Multiferroicity, Permittivity, Flexoelectricity, and Polar Nanoregions. *Condens. Matter* **2020**, *5* (4), No. 68.

(33) Kyung, W.; Kim, C. H.; Kim, Y. K.; Kim, B.; Kim, C.; Jung, W.; Kwon, J.; Kim, M.; Bostwick, A.; Denlinger, J. D.; Yoshida, Y.; Kim, C. Electric-Field-Driven Octahedral Rotation in Perovskite. *npj Quantum Mater.* **2021**, *6* (1), No. 5.

(34) Werner, V.; Aschauer, U.; Redhammer, G. J.; Schoiber, J.; Zickler, G. A.; Pokrant, S. Synthesis and Structure of the Double-Layered Sillén-Aurivillius Perovskite Oxychloride La2.1Bi2.9-Ti2O11Cl as a Potential Photocatalyst for Stable Visible Light Solar Water Splitting. *Inorg. Chem.* **2023**, *62* (17), 6649−6660.

(35) Li, L.; Han, Q.; Tang, L.; Zhang, Y.; Li, P.; Zhou, Y.; Zou, Z. Flux Synthesis of Regular Bi4TaO8Cl Square Nanoplates Exhibiting Dominant Exposure Surfaces of {001} Crystal Facets for Photocatalytic Reduction of CO2 to Methane. *Nanoscale* **2018**, *10* (4), 1905−1911.

(36) Gopakumar, A.; Ren, P.; Chen, J.; Rodrigues, B. V. M.; Ching, H. Y. V.; Jaworski, A.; Van Doorslaer, S.; Rokicińska, A.; Kuśtrowski, P.; Barcaro, G.; Monti, S.; Slabon, A.; Das, S. Lignin-Supported Heterogeneous Photocatalyst for the Direct Generation of H2O2from Seawater. *J. Am. Chem. Soc.* **2022**, *144* (6), 2603−2613.

(37) Zhang, G.; Cai, L.; Zhang, Y.; Wei, Y. Bi5+, Bi(3−x)+, and Oxygen Vacancy Induced BiOClxI1−x Solid Solution toward Promoting Visible-Light Driven Photocatalytic Activity. *Chem. - Eur. J.* **2018**, *24* (29), 7434−7444.

(38) Tao, X.; Shi, W.; Zeng, B.; Zhao, Y.; Ta, N.; Wang, S.; Adenle, A. A.; Li, R.; Li, C. Photoinduced Surface Activation of Semiconductor Photocatalysts under Reaction Conditions: A Commonly Overlooked Phenomenon in Photocatalysis. *ACS Catal.* **2020**, *10* (10), 5941−5948.

(39) Zhou, X.; Dong, H. Density Functional Studies on Layered Perovskite Oxyhalide Bi4MO8X Photocatalysts (M = Nb and Ta, X = Cl, Br, and I). *J. Phys. Chem. C* **2017**, *121* (38), 20662−20672.

(40) Ye, L.; Deng, Y.; Wang, L.; Xie, H.; Su, F. Bismuth-Based Photocatalysts for Solar Photocatalytic Carbon Dioxide Conversion. *ChemSusChem* **2019**, *12* (16), 3671−3701.

(41) Moun, M.; Vasdev, A.; Pujar, R.; Madhuri, K. P.; Mogera, U.; John, N. S.; Kulkarni, G. U.; Sheet, G. Enhanced Electrical Transport through Wrinkles in Turbostratic Graphene Films. *Appl. Phys. Lett.* **2021**, *119* (3), No. 033102.

(42) Jiang, Y.; Toe, C. Y.; Mofarah, S. S.; Cazorla, C.; Chang, S. L. Y.; Yin, Y.; Zhang, Q.; Lim, S.; Yao, Y.; Tian, R.; Wang, Y.; Zaman, T.; Arandiyan, H.; Andersson, G. G.; Scott, J.; Koshy, P.; Wang, D.; Sorrell, C. C. Efficient Cocatalyst-Free Piezo-Photocatalytic Hydrogen Evolution of Defective BaTiO3-x Nanoparticles from Seawater. *ACS Sustainable Chem. Eng.* **2023**, *11* (8), 3370−3389.

(43) Kusainova, A. M.; Stefanovich, S. Y.; Dolgikh, V. A.; Mosunov, A. V.; Hervoches, C. H.; Lightfoot, P. Dielectric Properties and Structure of Bi4NbO8Cl and Bi4TaO8Cl. *J. Mater. Chem.* **2001**, *11* (4), 1141−1145.